CHARACTERIZATION OF SINTERED SiC BY USING NDE

George Y. Baaklini
Structural Integrity Branch
NASA Lewis Research Center

ABSTRACT

Capabilities of projection microfocus x-radiography and of ultrasonic velocity and attenuation for characterizing silicon carbide specimens were assessed. Silicon carbide batches covered a range of densities and different microstructural characteristics. Room-temperature, four-point flexural strength tests were conducted. Fractography was used to identify types, sizes, and locations of fracture origins. Fracture toughness values were calculated from fracture strength and flaw characterization data. Detection capabilities of radiography for fracture-causing flaws were evaluated. Applicability of ultrasonics for verifying material strength and toughness was examined. Radiography proved useful in detecting high-density inclusions and isolated voids, but failed in detecting surface and subsurface agglomerates and large grains as fracture origins. Ultrasonic velocity dependency on density was evident. Attenuation dependency on density and mean pore size was clearly demonstrated. Understanding attenuation as a function of toughness was limited by shortcomings in K_{IC} determination.

SPECIMEN SINTERING AND HOT ISOSTATIC PRESSING CONDITIONS

Twenty-five modulus of rupture (MOR) bars were prepared from -100-mesh α-SiC powder containing boron and carbonaceous resin binders. Compaction of the green specimens included dry pressing the powder by using a double-action, tungsten-lined die, vacuum sealing the green bars in thin-wall latex tubing, and cold isopressing the bars at 420 MPa. These bars represent five different batches which were sintered or sintered and hot isostatically pressed (HP) in order to tailor their density and microstructure. All bars were machined, the four long edges beveled, and further polished to a 0.07-μm rms surface finish. Nominal test bar dimensions were 2.72 by 5.58 by 31.71 mm.

Batch number	Sintering			Hot isostatic pressing			Density, g/cm^3, ± 0.01 g/cm^3
	Temperature, °C	Time, hr	Argon pressure, MPa	Temperature, °C	Time, hr	Argon pressure, MPa	
1	2200	0.5	0.1	----	---	---	3.12
2HP	2200	1.5	↓	2100	0.5	138	3.14
4	2300	1.0		----	---	---	3.05
4HP	2300	1.0		2150	1.0	138	3.10
5HP	2100	.75		2100	1.0	138	2.92

CD-88-32633

MICROSTRUCTURAL CHARACTERIZATION

Mean pore size, shape, and orientation were determined from photomicrographs of polished representative samples from each batch by applying two-dimensional Fourier transform theory (Generazio, 1986). Mean grain size was determined from photomicrographs of polished and etched representative samples of each batch by using an interactive image analysis system where grain boundaries could be traced at a digitizer tablet.

Batch number	Density, g/cm^3	Mean grain size,[a] μm			Mean pore size,[a,b] μm			Grain shape
		Circle[c]	Ellipse[d]		Circle[e]	Ellipse[a,f]		
		Diameter	Major	Minor	Diameter	Major	Minor	
1	3.12	5.76	7.94	4.56	1.60	1.61	1.59	Equiaxed and elongated
2HP	3.14	6.75	9.61	5.15	1.63	1.75	1.50	Equiaxed and elongated
4	3.05	11.56	19.39	7.73	3.82	4.00	3.64	Elongated
4HP	3.10	11.18	18.08	7.82	3.44	3.60	3.27	Elongated
5HP	2.92	3.36	4.40	2.78	2.29	2.38	2.19	Equiaxed

[a] ±0.2 μm.
[b] No preferred orientation.
[c] Assuming all grains are equiaxed.
[d] Assuming all grains are elongated.
[e] Calculated average from f.
[f] Real measurements off the mean shape.

CD-88-32734

PULSE-ECHO ULTRASONICS OF MOR BARS

Velocity and attenuation measurements were determined for all samples through the thickness at three different locations in the highest stressed area of the test specimen. The pulse-echo technique, with a 100-MHz broadband longitudinal-wave transducer, was used to measure the cross correlation velocity (Hull et al., 1985) and the attenuation coefficient from the first and second back surface reflections. The front surface reflections obtained with and without the bar in place were used to calculate the reflection coefficient of the buffer rod-couplant-sample interface. This frequency-dependent reflection coefficient was incorporated for precision attenuation measurements (Generazio, 1985).

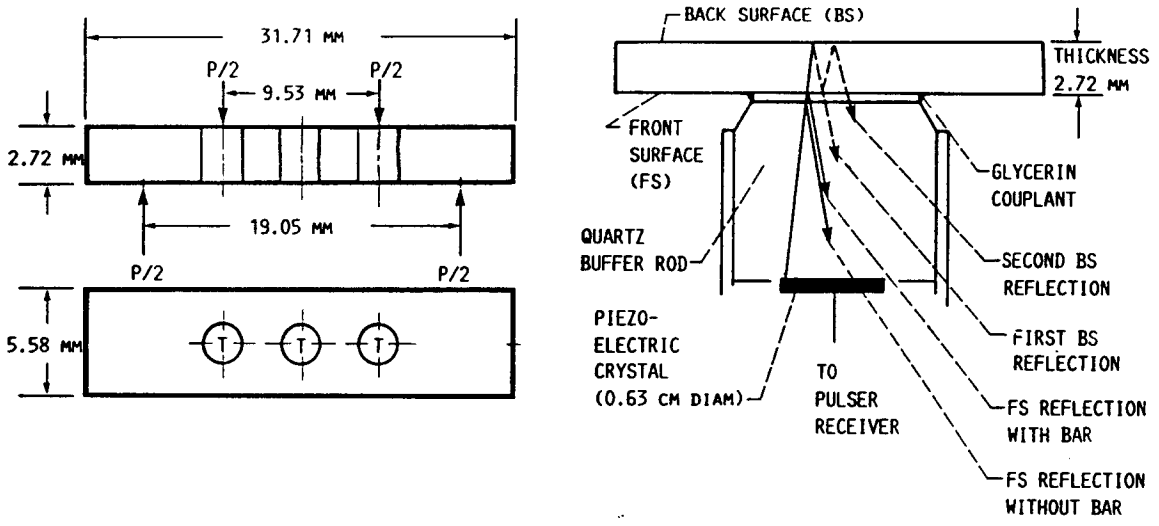

LOCATION OF TRANSDUCER FOR ULTRASONIC MEASUREMENTS IS DENOTED BY T, AND P IS APPLIED LOAD

CD-88-32735

RADIOGRAPHIC EVALUATION

All specimens were film radiographed in order to detect potential fracture-causing flaws. The microfocus system used was operated in the projection mode (x5 magnification) and in the 30 to 60 kV range with a beam current range of 0.25 to 0.32 mA. The system had a molybdenum anode and a 10-μm focal spot. All radiographs were manually developed, and were examined with the aid of a x7 optical measuring magnifier under variable-intensity backlighting (1000 to 9000 lm/m^2) in subdued room lighting. Test bars were radiographed in two modes, the (W,L) mode, where x rays were transmitted through the thickness, and the (T,L) mode, where x rays were transmitted through the width. When combined, they form a three-dimensional radiographic location of flaws.

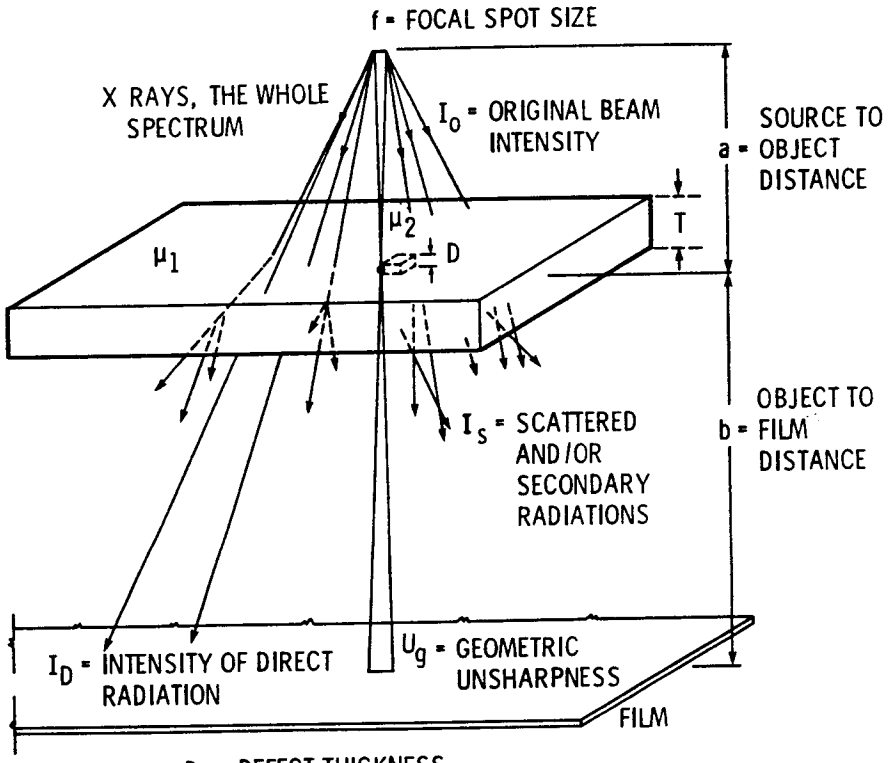

CD-88-32736

ASSESSMENT OF FRACTURE ORIGINS

Out of 25 specimens tested, 17 fracture origins were identifiable. The type, shape, size, and location of fracture origins are tabulated below. The 17 fracture origins identified were 5 bulk voids, 2 surface voids, 1 iron-rich inclusion, 1 large grain, 3 bulk agglomerates, and 5 surface agglomerates.

Batch number	Specimen number	Type	Shape	D,[a] μm	A[a] or 2A, μm	2C,[a] μm
1	3	Unidentified	----------	---	---	---
	5	Agglomerate	Circular	6	45	45
	8	Void	Irregular	14	69	69
	12	Agglomerate	Elliptical	60	40	70
	13	Void	Elliptical	40	80	104
2HP	2	Void	Semi-elliptical	0	19	67
	5	Agglomerate	Elliptical	12	65	127
	8	Void	Elliptical	120	58	92
	11	Unidentified	----------	---	---	---
	23	Agglomerate	Semi-elliptical	0	46	92
4	4	Void	Elliptical	50	69	127
	14	Void	Semi-elliptical	0	58	117
	15	Unidentified	----------	---	---	---
	16	Unidentified	----------	---	---	---
	18	Large Grain	Trapezoidal	7	34	58
4HP	1	Unidentified	----------	---	---	---
	5	Unidentified	----------	---	---	---
	8	Fe inclusion	Irregular	50	140	140
	9	Unidentified	----------	---	---	---
	24	Unidentified	----------	---	---	---
5HP	35	Agglomerate	Semi-elliptical	0	50	150
	36	Agglomerate	Irregular	0	35	55
	37	Agglomerate	Semicircular	0	30	200
	46	Void	Elliptical	120	100	120
	59	Agglomerate	Circular	0	60	60

[a]See sketch below.

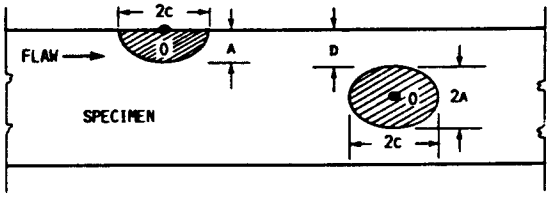

CD-88-32737

Shown below are scanning electron micrographs typical of fracture origins in sintered SiC MOR bars:

BULK VOID

SURFACE AGGLOMERATE

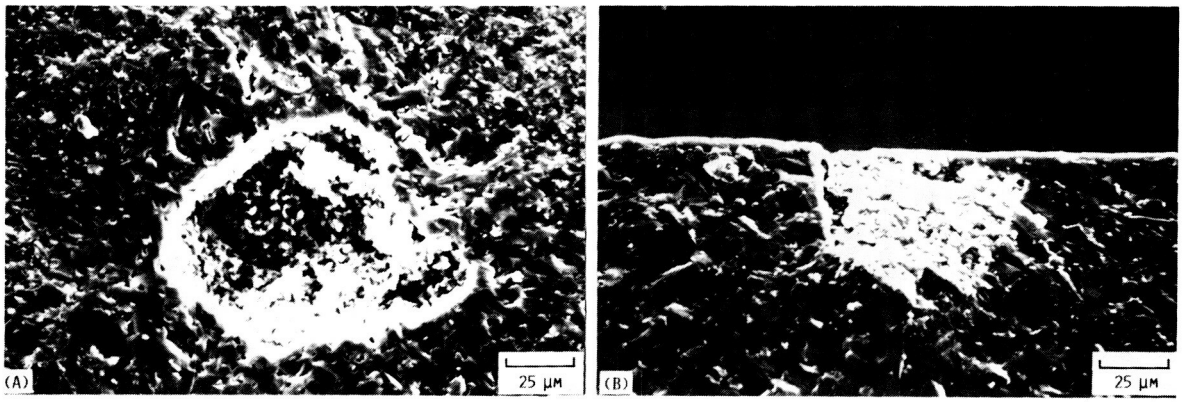

CD-88-32738

BULK VOID (AGGLOMERATE-LIKE)

LARGE GRAIN

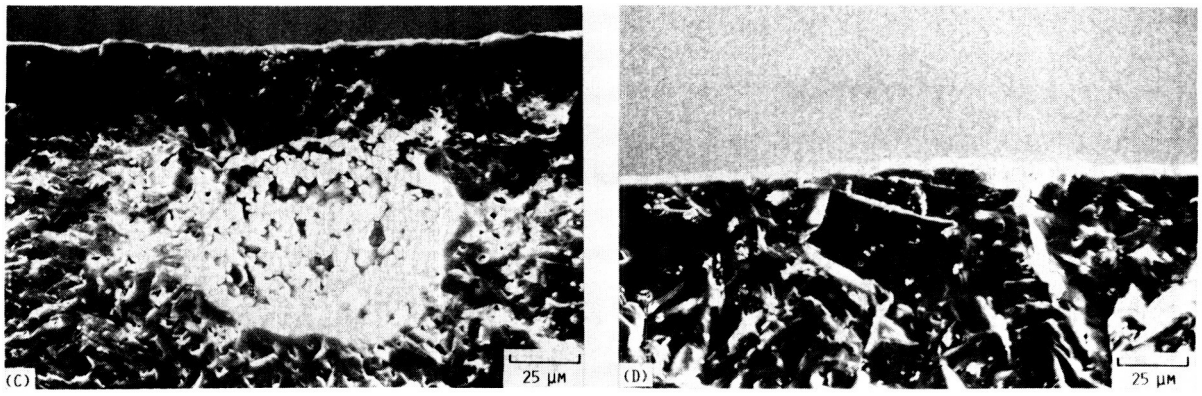

CD-88-32739

RADIOGRAPHIC DETECTION OF FRACTURE ORIGINS

Seven out of seventeen identified fracture origins were radiographically detected. All five bulk voids, one out of two surface voids, and the iron-rich inclusion, were detected. All surface and subsurface agglomerates and the large grain were missed. In general, the flaw size as it appeared on the radiograph was less than or equal to its real size as determined optically.

Batch number	Specimen number	Type[a]	Optical flaw dimensions, μm		Sensitivity,[b] percent		Flaw detected		Radiographic flaw dimensions, μm	
			XT	XW	T	W	T	W	XW, XL	XT, XL
1	3	U	---	---	---	---	---	---	--------	--------
	5	BA	45	45	1.6	0.8	No	No	--------	--------
	8	BV	69	69	2.5	1.2	Yes	Yes	43, 85	43, 85
	12	BA	40	70	1.4	1.3	No	No	--------	--------
	13	BV	80	104	2.9	1.9	Yes	No	43, 43	--------
2HP	2	SV	19	67	0.7	1.2	No	No	--------	--------
	5	BA	65	127	2.4	2.3	No	No	--------	--------
	8	BV	58	92	2.1	1.7	Yes	No	63, 43	--------
	11	U	---	---	---	---	---	---	--------	--------
	23	SA	46	92	1.7	1.6	No	No	--------	--------
4	4	BV	69	127	2.5	2.3	Yes	No	105, 105	--------
	14	SV	58	115	2.1	1.6	Yes	Yes	105, 42	42, 105
	15	U	---	---	---	---	---	---	--------	--------
	16	U	---	---	---	---	---	---	--------	--------
	18	LG	34	58	1.2	1.0	No	No	--------	--------
4HP	1	U	---	---	---	---	---	---	--------	--------
	5	U	---	---	---	---	---	---	--------	--------
	8	FeI	140	140	5.3	2.5	Yes	Yes	62, 62	62, 62
	9	U	---	140	---	---	---	---	--------	--------
	24	U	---	140	---	---	---	---	--------	--------
5HP	35	SA	50	150	1.8	2.7	No	No	--------	--------
	36	SA	35	55	1.3	1.0	No	No	--------	--------
	37	SA	130	200	4.8	3.6	No	No	--------	--------
	46	BV	100	120	3.8	2.2	Yes	Yes	106, 64	106, 64
	59	SA	60	60	2.2	1.1	No	No	--------	--------

[a]U, unidentified; BA, bulk agglomerate; BV, bulk void; SA, surface agglomerate; SV, surface void; LG, large grain; FeI, iron inclusion.
[b]Sensitivity, 100(XT/T) or 100(XW/W).

[Specimen dimensions measured along thickness, T, width, W, and length, L. Flaw dimensions XT, XW, and XL measured along T, W, and L, respectively.]

CD-88-32740

FLEXURAL STRENGTH AND FRACTURE TOUGHNESS RESULTS

Fracture toughness (K_{IC}) values were obtained from the relationship between fracture strength and flaw shape, size, and location based on the work by Brown and Srawley (1967), Evans and Tapin (1972), Bansal (1976), Bansal and Duckworth (1977), and Danforth and Richman (1983).

There is no reason to believe, on the basis of an f-test at the 95-percent confidence level (Natrella, 1963), that the five batches differ in strength variability. Further, there is only reason to believe that the mean strength for batch 1 exceeds that of batch 4HP; otherwise no differences in mean strengths of all other batches are noted. This is substantiated by a t-test at the 95-percent confidence level.

On the basis of an f- and t-test at the 95-percent confidence level, none of the four batches differed in toughness variability or in mean toughness.

Batch number	Specimen number	Fracture strength of tensile surface, σ_t, MPa	Fracture strength at origin, σ_f, MPa	$(\sigma_t)_{avg}$, standard deviation, MPa	Y/Z	Fracture toughness, K_{IC}, MN·m$^{-3/2}$	$(K_{IC})_{avg}$, standard deviation, MN·m$^{-3/2}$
1	3	356	---	338±48	---	---	3.26±0.26
	5	389	385		1.27	3.23	
	8	269	265		1.27	2.80	
	12	382	369		1.42	3.31	
	13	326	317		1.31	3.71	
2HP	2	319	319	319±52	1.60	2.23	2.88±0.65
	5	211	267		1.67	3.59	
	8	322	305		1.40	3.25	
	11	402	---		---	---	
	23	281	281		1.27	2.42	
4	4	265	256	315±40	1.44	3.06	3.22±0.39
	14	304	304		1.27	2.94	
	15	342	---		---	---	
	16	366	---		---	---	
	18	296	281		1.60	3.67	
4HP	1	251	---	273±51	---	---	---------
	5	334	---		---	---	
	8	209	201		---	---	
	9	306	---		---	---	
	24	271	---		---	---	
5HP	35	289	289	297±25	1.56	3.19	3.20+0.73
	36	324	324		1.25	2.40	
	37	288	288		1.25	4.10	
	46	319	298		1.26	3.75	
	59	264	264		1.26	2.57	

CD-88-32741

ULTRASONIC VELOCITY AND BULK DENSITY

Average velocity based on three measurements at different locations in the MOR bar was plotted as a function of bulk density for all 25 bars. The data show that velocity is an increasing function of density. The average velocities are 1.184, 1.188, 1.169, 1.189 and 1.099 cm/μs for batches 1, 2HP, 4, 4HP, and 5HP, respectively. By comparing these results with corresponding average bulk densities, there is approximately a 1-percent change in velocity for a 1-percent change in density.

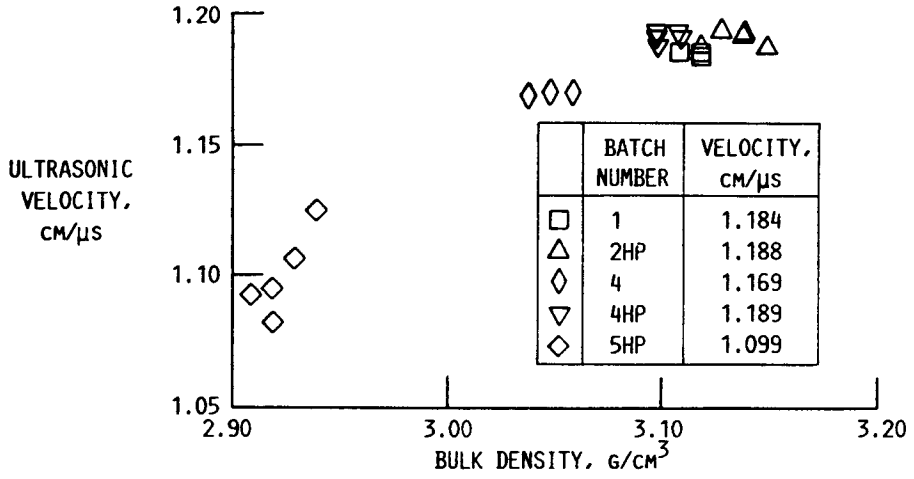

CD-88-32742

ULTRASONIC ATTENUATION, FLEXURAL STRENGTH, AND FRACTURE TOUGHNESS

Attenuation coefficient results are plotted as a function of frequency for all five batches. Plotted data are the measured attenuation at or very near the location where fracture took place. Dashed lines represent the upper and lower boundaries of the data of each batch of specimens. Attenuation coefficient in the frequency regime shown does differentiate substantially between batches on the basis of their density and microstructural characteristics. Attenuation dependency on density can be seen by comparing batch 4 and batch 4HP attenuation data, where a 1.6-percent difference in density (also a 1-percent difference in velocity) reflects a 56-percent difference in attenuation at a frequency of 100 MHz. Knowing a priori that attenuation is not due to grain boundary-scattering mechanism (Generazio, 1987), the attenuation data for batches 5HP, 4, and 1 therefore demonstrate the attenuation dependency on density and average pore size.

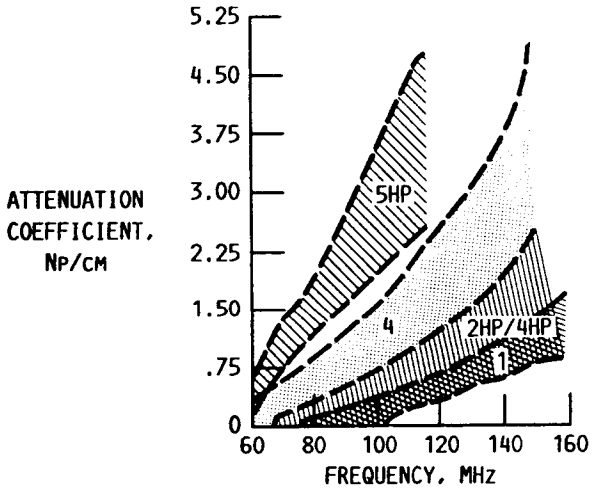

BATCH NUMBER	DENSITY, G/CM^3	MEAN PORE DIAMETER, μM	FLEXURAL STRENGTH, MPA	FRACTURE TOUGHNESS, $MN \cdot M^{-3/2}$
1	3.12	1.60	338±48	3.26±0.37
2HP	3.14	1.63	319±52	2.88±0.65
4	3.05	3.82	315±40	3.22±0.39
4HP	3.10	3.44	273±51	---------
5HP	2.92	2.38	297±25	3.20±0.73

CD-88-32743

CONCLUSIONS

1. Radiography proved useful in detecting high-density inclusions and isolated voids, but failed in detecting surface and subsurface agglomerates and large grains as fracture origins.

2. Ultrasonic dependency on velocity was evident.

3. Attenuation dependency on density and mean pore size was clearly demonstrated.

4. Understanding attenuation as a function of toughness was limited, first, by the fact that one dominant flaw can mask the effect of bulk porosity and microstructure on strength and toughness and, second, by shortcomings in K_{IC} determination.

REFERENCES

Bansal, G.K., 1976, "Effect of Flaw Shape on Strength of Ceramics," J. Am. Ceram. Soc., 59 [1-2] 87-88.

Bansal, G.K., and Duckworth, W.H., 1977, "Fracture Stress as Related to Flaw and Fracture Mirror Sizes," J. Am. Ceram. Soc., 60 [7-8] 304-310.

Brown, W.F., Jr., and Srawley, J.E., 1967, Plane Strain Crack Toughness Testing of High Strength Metallic Materials. ASTM-STP-410, ASTM, Philadelphia, PA, pp. 1-15.

Danforth, S.C., and Richman, M.H., 1983, "Strength and Fracture Toughness of Reaction-Bonded Si_3N_4," Am. Ceram. Soc. Bull., 62 [4] 501-505.

Evans, A.G., and Tapin, G., 1972, "Effects of Microstructure on the Stress to Propagate Inherent Flaws," Proc. Br. Ceram. Soc., No. 20, 275-297.

Generazio, E.R., 1985, "The Role of the Reflection Coefficient in Precision Measurement of Ultrasonic Attenuation," Mater. Eval., 43 [8] 995-1004.

Generazio, E.R., 1986, "Determination of Grain Size Distribution Function Using Two-Dimensional Fourier Transforms of Tone Pulse Encoded Images," NASA TM-88790.

Generazio, E.R., Roth, D.J., and Baaklini, G.Y., 1987, "Imaging Subtle Microstructural Variations in Ceramics with Precision Ultrasonic Velocity and Attenuation Measurements," NASA TM-100129.

Hull, D.R., Kautz, H.E., and Vary, A., 1985, "Measurement of Ultrasonic Velocity Using Phase-Slope and Cross-Correlation Methods," Mater. Eval., 43 [11] 1455-1460.

Natrella, M.G., 1963, Experimental Statistics. NBS Handbook No. 91, National Bureau of Standards, Washington, D.C.

C-2